The EMBO Journal (2011) 30, 719–730 | © 2011 European Molecular Biology Organization | Some Rights Reserved 0261-4189/11
www.embojournal.org

THE EMBO JOURNAL

EMBO open

PICK1 inhibition of the Arp2/3 complex controls dendritic spine size and synaptic plasticity

Yasuko Nakamura[1], Catherine L Wood[1,2,3], Andrew P Patton[2,3], Nadia Jaafari[1], Jeremy M Henley[1], Jack R Mellor[2] and Jonathan G Hanley[1,*]

[1]MRC Centre for Synaptic Plasticity, School of Biochemistry, University of Bristol, University Walk, Bristol, UK and [2]MRC Centre for Synaptic Plasticity, School of Physiology and Pharmacology, University of Bristol, University Walk, Bristol, UK

Activity-dependent remodelling of dendritic spines is essential for neural circuit development and synaptic plasticity, but the precise molecular mechanisms that regulate this process are unclear. Activators of Arp2/3-mediated actin polymerisation are required for spine enlargement; however, during long-term depression (LTD), spines shrink via actin depolymerisation and Arp2/3 inhibitors in this process have not yet been identified. Here, we show that PICK1 regulates spine size in hippocampal neurons via inhibition of the Arp2/3 complex. PICK1 knockdown increases spine size, whereas PICK1 overexpression reduces spine size. NMDA receptor activation results in spine shrinkage, which is blocked by PICK1 knockdown or overexpression of a PICK1 mutant that cannot bind Arp2/3. Furthermore, we show that PICK1–Arp2/3 interactions are required for functional hippocampal LTD. This work demonstrates that PICK1 is a novel regulator of spine dynamics. Via Arp2/3 inhibition, PICK1 has complementary yet distinct roles during LTD to regulate AMPA receptor trafficking and spine size, and therefore functions as a crucial factor in both structural and functional plasticity.

The EMBO Journal (2011) **30,** 719–730. doi:10.1038/emboj.2010.357; Published online 21 January 2011
Subject Categories: cell & tissue architecture; neuroscience
Keywords: actin; AMPA receptor; cytoskeleton; dendritic spine; synapse

Introduction

Long-term synaptic plasticity is thought to underlie learning and memory and also the tuning of neural circuitry during development. Two major postsynaptic processes are involved in plasticity of excitatory synapses: modification of AMPA receptors (AMPARs), which mediate the majority of fast synaptic excitation in the brain, and alterations in the size and shape of dendritic spines. These protrusions from the dendritic shaft compartmentalise the postsynaptic apparatus, and concentrate biochemical signals such as calcium (Kennedy *et al*, 2005; Bloodgood and Sabatini, 2007). During long-term depression (LTD), dendritic spines shrink and the number of AMPARs expressed at the synapse is decreased via regulated trafficking. Conversely, long-term potentiation (LTP) involves spine growth and an increase in synaptic AMPAR number (Matsuzaki, 2007; Shepherd and Huganir, 2007).

The dynamic actin cytoskeleton is central to the regulation of cell morphology and vesicle trafficking by exerting mechanical forces that alter the shape of the plasma membrane (Merrifield, 2004; Kaksonen *et al*, 2006). Actin dynamics have a major role in determining spine structure (Dillon and Goda, 2005; Sekino *et al*, 2007), and have also been suggested to regulate the functional expression of LTD and LTP (Cingolani and Goda, 2008). During LTD, actin dynamics in spines shift from filamentous (F-) actin towards monomeric globular (G-) actin, suggesting that actin polymerisation is inhibited during this process (Okamoto *et al*, 2004). The Arp2/3 complex is the major catalyst for the formation of branched actin networks that mediate changes in membrane geometry and is concentrated in dendritic spines (Takenawa and Suetsugu, 2007; Racz and Weinberg, 2008; Rocca *et al*, 2008). The Arp2/3 activators N-WASP, WAVE and cortactin stimulate actin polymerisation and have all been implicated in spine morphogenesis (Hering and Sheng, 2003; Kim *et al*, 2006; Wegner *et al*, 2008). However, inhibitors of Arp2/3-mediated actin polymerisation involved in spine morphology and in functional LTD have not yet been identified.

An important unresolved question is whether spine dynamics and AMPAR trafficking are linked during functional synaptic plasticity. As actin regulation is involved in both processes, there is the intriguing possibility that specific regulators of actin polymerisation may regulate both receptor trafficking and spine morphology.

PICK1 is a PDZ and BAR domain containing protein that binds AMPAR subunits GluA2/3 (Hanley, 2008). This interaction is required for AMPAR internalisation in response to Ca^{2+} influx via NMDAR activation in hippocampal neurons during LTD (Kim *et al*, 2001; Hanley and Henley, 2005; Terashima *et al*, 2008). We recently demonstrated that PICK1 directly binds to and inhibits the activity of the Arp2/3 complex, and that this has a central role in AMPAR trafficking in hippocampal neurons (Rocca *et al*, 2008).

In this study, we show that PICK1 restricts spine size under basal conditions via direct interaction with the Arp2/3

*Corresponding author. MRC Centre for Synaptic Plasticity, School of Biochemistry, Medical Sciences Building, University of Bristol, University Walk, Bristol BS8 1TD, UK. Tel.: +44 117 331 1944; Fax: +44 117 929 1687; E-mail: jon.hanley@bristol.ac.uk
[3]These authors contributed equally to this work

Received: 14 May 2010; accepted: 20 December 2010; published online: 21 January 2011

complex. PICK1–Arp2/3 interactions are required for spine shrinkage during chemical LTD, and also for LTD of synaptic transmission.

Results

PICK1 expression regulates spine size via interaction with Arp2/3

To investigate the role of PICK1 in regulating dendritic spine size, we used transfection of IRES plasmids that express both PICK1 and actin^{EGFP}. Actin^{EGFP} localises to dendritic spines and is therefore an amenable marker to measure spine size (Ackermann and Matus, 2003; Chao *et al*, 2008; Saneyoshi *et al*, 2008). Actin^{EGFP}-positive spines are much more defined than those expressing EGFP, facilitating analysis. In addition, actin^{EGFP}-positive spines are detectable even when the spine head is in the same *xy* position as the dendritic shaft, whereas those expressing unconjugated EGFP would be obscured.

Expression of WT-PICK1-IRES-actin^{EGFP} in dissociated hippocampal pyramidal neurons results in reduced dendritic spine size compared with neurons expressing control-IRES-actin^{EGFP} (Figure 1A; control $1.74 \pm 0.05\,\mu m^2$, WT-PICK1 $1.40 \pm 0.04\,\mu m^2$, $P<0.001$). To investigate the role of Arp2/3 inhibition, we made use of a single-point mutation in PICK1, W413A, which specifically blocks the Arp2/3 interaction and Arp2/3 inhibition by PICK1 (Rocca *et al*, 2008). This mutation blocks the reduction in spine size, indeed expression of W413A-PICK1-IRES-actin^{EGFP} results in larger spines (Figure 1; W413A-PICK1 $1.94 \pm 0.05\,\mu m^2$, $P<0.05$). Overexpression of neither WT-PICK1 nor W413A-PICK1 influenced the number of spines compared with controls (Figure 1A). We tested both IRES-actin^{EGFP} and IRES-EGFP constructs, and obtained the same result (Supplementary Figure S1). We extended this analysis and measured spine length using NeuronStudio (Rodriguez *et al*, 2008). WT-PICK1 overexpression causes a significant reduction in spine length, and

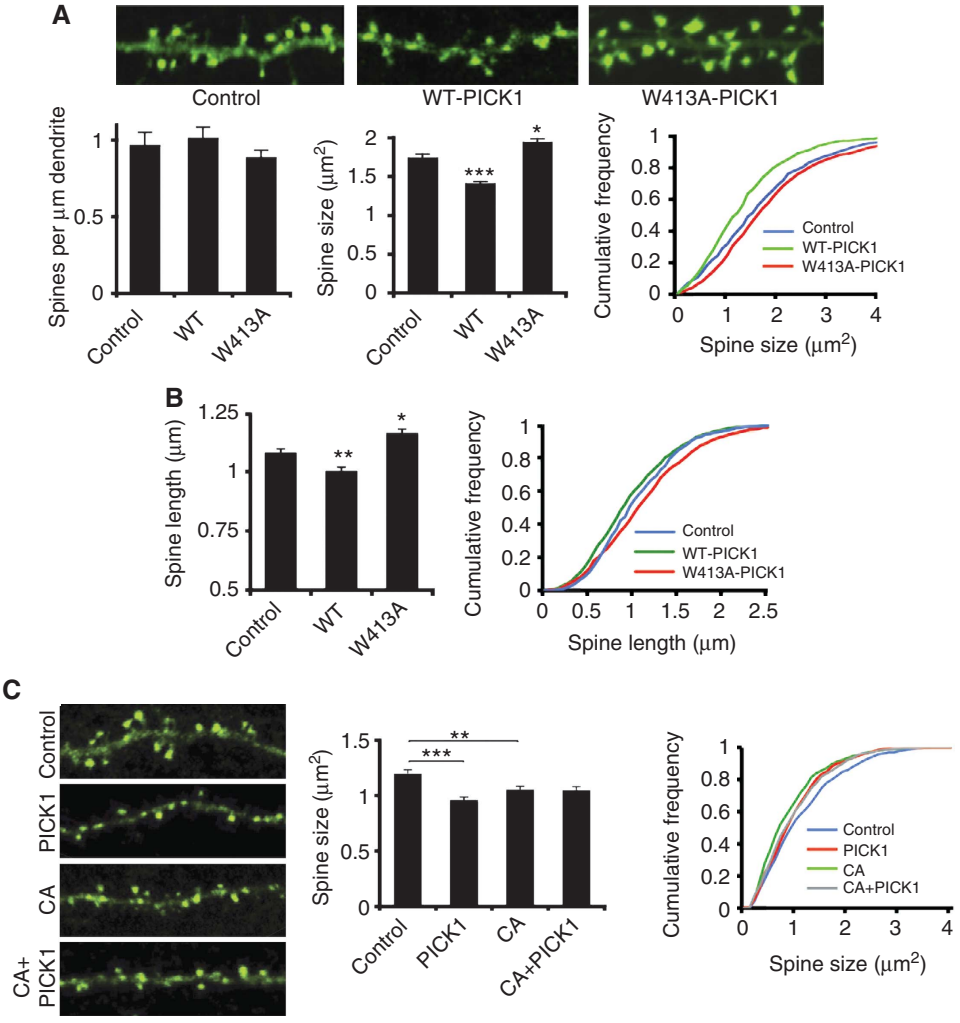

Figure 1 PICK1 overexpression leads to spine shrinkage via its interaction with the Arp2/3 complex. (**A**) Analysis of spine size based on cross-sectional area. Top panels show representative images of dendrites from cultured hippocampal neurons transfected with control-IRES-actin^{EGFP}, WT-PICK1-IRES-actin^{EGFP} or W413A-PICK1-IRES-actin^{EGFP}. Image width is 20 µm. Graphs show quantification of linear spine densities and spine size. $^{*}P<0.05$, $^{***}P<0.001$ compared with control, K–S test. (**B**) Analysis of spine length. Graphs show quantification of one-dimensional length for spines on neurons transfected with control-IRES-EGFP, WT-PICK1-IRES-EGFP or W413A-PICK1-IRES-EGFP. $^{*}P<0.05$, $^{**}P<0.005$ compared with control, K–S test. (**C**) Inhibition of Arp2/3 activity by N-WASP CA domain mimics and occludes spine shrinkage by PICK1 overexpression. Top panels show representative images from cultured hippocampal neurons transfected with either mCherry–CA or mCherry control and either control-IRES-actin^{EGFP} or WT-PICK1-IRES-actin^{EGFP} (only actin^{EGFP} channel is shown). Image width is 20 µm. Graphs show quantification of spine size. $^{**}P<0.01$, $^{***}P<0.001$, K–S test.

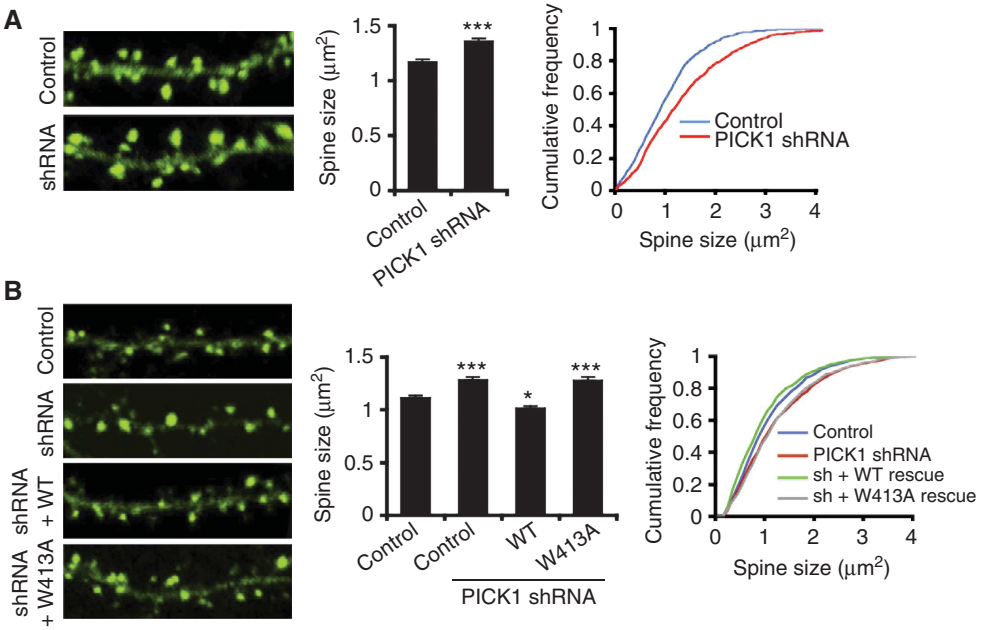

Figure 2 Endogenous PICK1 restricts spine size via its interaction with the Arp2/3 complex. (**A**) Knockdown of endogenous PICK1 expression results in increased spine size. Left panels show representative images of dendrites from neurons transfected with actin^{EGFP} and either control-mCherry or PICK1 shRNA–mCherry plasmids. Only actin^{EGFP} channel is shown. Image width is 20 μm. Graphs show quantification of spine size. ***$P<0.001$ compared with control, K–S test. (**B**) Co-expression of WT-PICK1 rescues shRNA-induced spine enlargement, W413A-PICK1 does not. Left panels show representative images of dendrites from neurons transfected with either control-mCherry or PICK1 shRNA–mCherry plasmids and sh-resistant WT-PICK1-IRES-actin^{EGFP}, sh-resistant W413A-PICK1-IRES-actin^{EGFP} or control-IRES-actin^{EGFP}. Only actin^{EGFP} channel is shown. Image width is 20 μm. Graphs show quantification of spine size. *$P<0.05$, ***$P<0.001$ compared with control, K–S test.

W413A-PICK1 overexpression causes a significant increase in spine length compared with controls (control 1.08 ± 0.02 μm, WT-PICK1 1.00 ± 0.01 μm, $P<0.005$, W413A-PICK1 1.16 ± 0.02 μm, $P<0.05$; Figure 1B). To provide further evidence that PICK1 shrinks spines via Arp2/3 inhibition, we utilised the CA domain of N-WASP, which is a well-established inhibitor of Arp2/3 activity, and leads to spine shrinkage when expressed in cultured neurons (Rohatgi *et al*, 1999; Haeckel *et al*, 2008). These experiments confirm this effect on spine size, and show that mCherry–CA expression in cultured neurons results in a significant reduction in spine size compared with mCherry controls (control 1.20 ± 0.03 μm^2, CA 1.05 ± 0.03 μm^2, $P<0.01$; Figure 1C). If PICK1 shrinks spines via Arp2/3 inhibition, CA overexpression and PICK1 overexpression should be mutually occluding with respect to spine shrinkage. In neurons co-expressing unconjugated mCherry, expression of WT-PICK1-IRES-actin^{EGFP} results in spine shrinkage compared with control-IRES-actin^{EGFP} (control 1.20 ± 0.03 μm^2, PICK1 0.96 ± 0.03 μm^2, $P<0.001$; Figure 1C). In contrast, in neurons co-expressing mCherry–CA, WT-PICK1-IRES-actin^{EGFP} expression has no effect on spine size compared with control-IRES-actin^{EGFP} (CA 1.05 ± 0.03 μm^2, CA + PICK1 1.05 ± 0.03 μm^2; Figure 1C). This demonstrates that inhibition of Arp2/3 activity via a distinct method (N-WASP CA domain) mimics and occludes the spine size phenotype of WT-PICK1 overexpression, supporting an Arp2/3 inhibitory mechanism for PICK1 in the regulation of spine size.

To analyse the role of endogenous PICK1 expression in the regulation of spine size, we employed shRNA-mediated knockdown to reduce PICK1 expression. We used an shRNA sequence that leads to 53% knockdown of PICK1 expressed in COS cells, or 47% of endogenous PICK1 5 days after transfection in neurons (Supplementary Figure S2).

Transfection of dissociated cultured neurons with plasmids encoding PICK1 shRNA results in a significant increase in spine size (Figure 2A; control 1.17 ± 0.03 μm^2, shRNA 1.36 ± 0.03 μm^2, $P<0.001$), but has no effect on the number of spines (data not shown). This demonstrates that endogenous PICK1 functions to restrict spine size under basal conditions.

To validate the specificity of the PICK1 shRNA, we generated shRNA-resistant rescue constructs for co-transfection with PICK1 shRNA. Expression of shRNA-resistant WT- or W413A-PICK1 in conjunction with knockdown of endogenous PICK1 by shRNA results in PICK1 expression levels that are 40% higher than endogenous PICK1 (Supplementary Figure S2B). Co-expression of shRNA-resistant WT-PICK1 causes a significant reduction in spine size compared with expression of PICK1 shRNA alone, demonstrating a rescue of the shRNA-induced phenotype. In fact, spines in these neurons were smaller than the control condition, indicating a small, but significant 'over-rescue' (Figure 2B; control 1.11 ± 0.02 μm^2, shRNA 1.29 ± 0.03 μm^2, shRNA + WT-PICK1 1.01 ± 0.02 μm^2, $P<0.001$ compared with shRNA, $P<0.05$ compared with control). This is consistent with the observed overexpression of PICK1 following co-transfection of PICK1 shRNA and sh-resistant rescue constructs. In contrast, co-expression of W413A-PICK1 does not rescue the shRNA-induced increase in spine size (shRNA + W413A-PICK1 1.28 ± 0.03 μm^2, $P>0.1$ compared with shRNA, $P<0.001$ compared with control) confirming the crucial role of PICK1–Arp2/3 interactions in restricting spine size. Taken together, these results demonstrate that PICK1 regulates spine

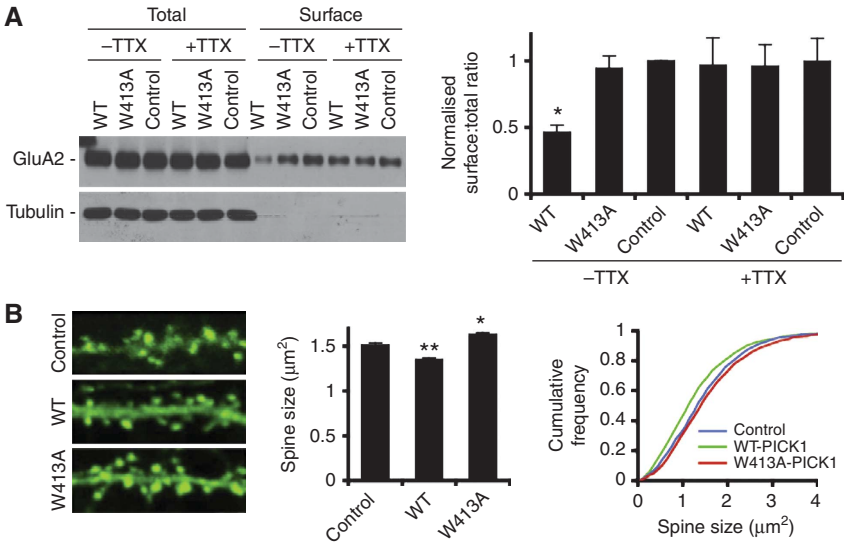

Figure 3 PICK1-mediated spine shrinkage occurs independently of GluA2 trafficking. (**A**) PICK1-mediated reduction in surface GluA2 is blocked by TTX. Hippocampal cultures were transduced with either control-IRES-EGFP, WT-PICK1-IRES-EGFP or W413A-PICK1-IRES-EGFP virus. Cultures were either treated with 0.5 μM TTX for 1 h or left untreated. Top panel shows representative western blot of 50% total GluA2 present in lysates and 100% surface (biotinylated) GluA2 after treatment. Graph shows pooled data presented as ratios of surface over total GluA2. $n=7$, $^{*}P<0.05$, *t*-test. (**B**) PICK1-mediated reduction in spine size persists in the presence of TTX. Experiment was carried out as in Figure 1 (A), except that 0.5 μM TTX was applied 1 h prior to cell fixation. $^{*}P<0.05$, $^{**}P<0.01$ compared with control, K–S test.

size under basal conditions via direct interaction with the actin-nucleating Arp2/3 complex.

PICK1-induced reduction in spine size is not caused by reduced surface GluA2, and does not involve PKC

It has been suggested that the level of GluA2 expressed at the synaptic plasma membrane regulates dendritic spine size (Passafaro *et al*, 2003; Hsieh *et al*, 2006; Saglietti *et al*, 2007). However, a number of reports also argue against this idea (Wang *et al*, 2007; Biou *et al*, 2008; Lu *et al*, 2009). Since PICK1 overexpression reduces surface levels of GluA2 (Terashima *et al*, 2004), a possible explanation for the reduced spine size following PICK1 overexpression could be that spine shrinkage occurs downstream of GluA2 internalisation. To address this, we utilised the observation that reduced surface GluA2 following PICK1 overexpression is activity dependent (Hanley and Henley, 2005; Terashima *et al*, 2008). Using surface biotinylation assays, we show that inhibition of synaptic activity using TTX blocks PICK1-mediated GluA2 internalisation (Figure 3A). Interestingly, PICK1 overexpression results in reduced spine size even in the presence of TTX (Figure 3B). Furthermore, while W413A-PICK1 expression increases spine size, it has no effect on surface GluA2 levels (Figure 3A and B). This demonstrates that PICK1 can regulate spine size independently of GluA2 trafficking, strongly suggesting that PICK1-induced spine shrinkage occurs via downregulation of structural F-actin in spines.

PICK1 specifically binds activated PKC and is involved in targeting this enzyme to dendritic spines (Staudinger *et al*, 1995; Perez *et al*, 2001). We therefore investigated whether PKC activation is involved in PICK1-mediated spine shrinkage using pharmacological inhibition of PKC. Application of the PKC inhibitor chelerythrine for 1 h before fixation has no effect on spine shrinkage induced by PICK1 overexpression (Supplementary Figure S3A). In addition, PKC activation by PMA has been shown to reduce spine size (Calabrese and Halpain, 2005). We therefore asked whether endogenous PICK1 is required for this process by carrying out live time lapse imaging of spines exposed to PMA (Supplementary Figure S3B). PKC activation causes a reduction in spine size 20–50 min following the initiation of drug application. PICK1 knockdown by shRNA has no effect on this process (Supplementary Figure S3B), indicating that PICK1 is not required for PKC-induced spine shrinkage. These results demonstrate that PKC and PICK1 do not functionally interact in the regulation of dendritic spine size.

PICK1–Arp2/3 interactions are involved in LTD-induced spine shrinkage

To study the role of PICK1 in dendritic spine shrinkage associated with LTD, we analysed spines following exposure to a chemical LTD protocol in hippocampal cultures. Bath application of 20 μM NMDA plus 20 μM glycine stimulates a significant spine shrinkage (Figure 4A; vehicle control $1.15\pm0.02\,\mu m^2$, NMDA $0.95\pm0.02\,\mu m^2$, $P<0.001$). This effect is similar in magnitude as observed in a report of LTD-induced reduction in spine size in hippocampal slices (Wang *et al*, 2007). Using this stimulus, we saw no significant change in the density of spines on the dendrite (Figure 4A).

Since PICK1 overexpression mimics NMDA-induced spine shrinkage (compare Figures 1 and 4A), we investigated whether these treatments mutually occlude. In agreement with this hypothesis, NMDAR activation has no effect on spine size in neurons transfected with WT-PICK1-IRES-actin^{EGFP}, suggesting that NMDA-induced spine shrinkage involves PICK1 (Figure 4B; control + vehicle $1.52\pm0.02\,\mu m^2$, control + NMDA $1.26\pm0.02\,\mu m^2$, $P<0.001$. WT-PICK1 + vehicle $1.22\pm0.01\,\mu m^2$, WT-PICK1 + NMDA 1.20 ± 0.01, $P=0.34$).

To specifically investigate the role of PICK1–Arp2/3 interactions in spine shrinkage, we analysed the effect of chemical

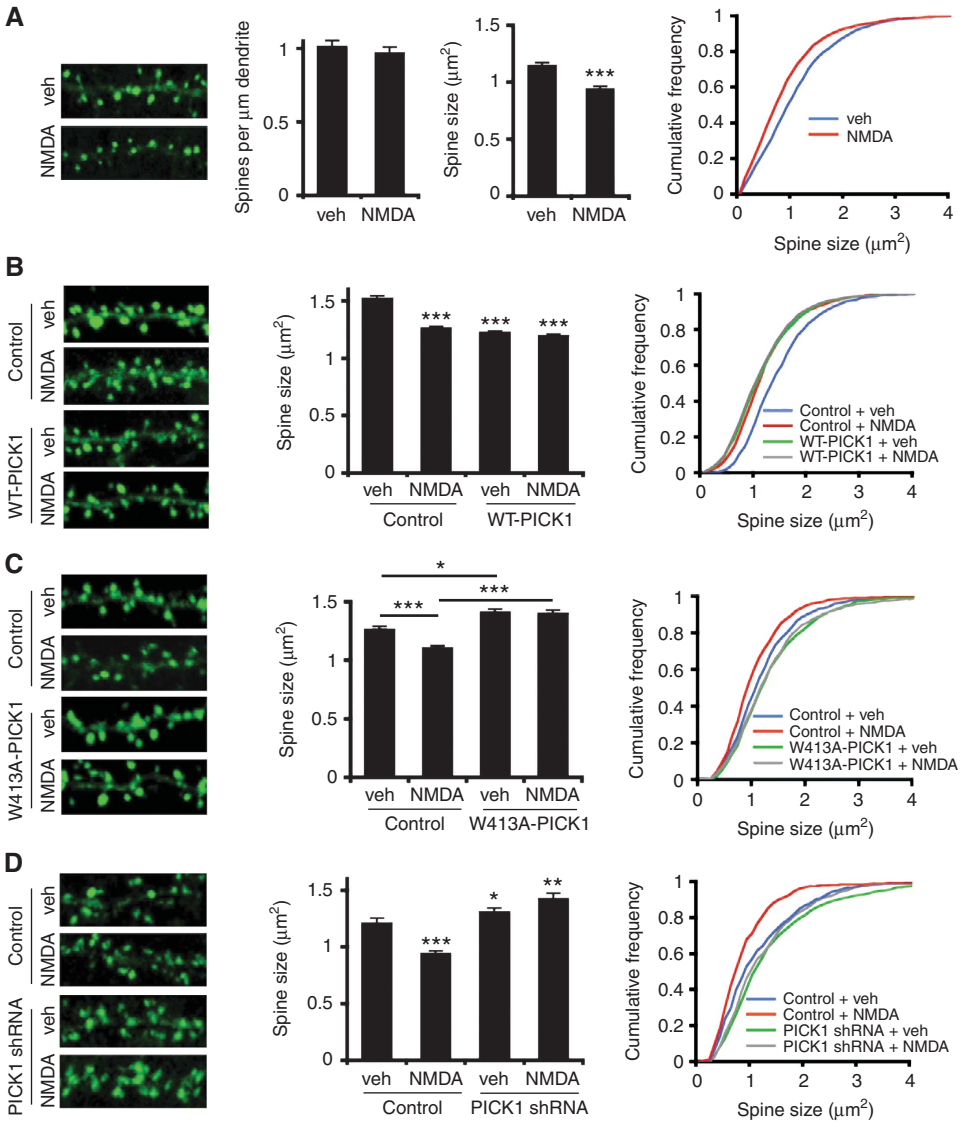

Figure 4 PICK1 mediates spine shrinkage following NMDAR activation via its interaction with the Arp2/3 complex. (**A**) NMDAR activation induces dendritic spine shrinkage. Left panels show representative images of dendrites from neurons treated with 20 μM NMDA, 20 μM glycine for 2 min (chemical LTD), followed by return to normal medium. Image width is 20 μm. Graphs show quantification of linear spine densities and spine area. ***$P<0.001$ compared with control, K–S test. (**B**) WT-PICK1 overexpression mimics and occludes chem-LTD-induced spine shrinkage. Left panels show representative images of dendrites from neurons expressing control-IRES-actin^{EGFP} or WT-PICK1-IRES-actin^{EGFP} and subjected either to NMDAR activation or vehicle control. Image width is 20 μm. Graphs show quantification of spine area. ***$P<0.001$ compared with control, K–S test. (**C**) W413A-PICK1-IRES-actin^{EGFP} expression inhibits chem-LTD-induced spine shrinkage. Left panels show representative images of dendrites from neurons expressing control-IRES-actin^{EGFP} or W413A-PICK1-IRES-actin^{EGFP} and subjected either to NMDAR activation or vehicle control. Image width is 20 μm. Graphs show quantification of spine area. *$P<0.05$, ***$P<0.001$, K–S test. (**D**) Endogenous PICK1 is required for chem-LTD-induced spine shrinkage. Left panels show representative images of dendrites from neurons expressing control-IRES-actin^{EGFP} and either PICK1 shRNA–mCherry or control-mCherry and subjected either to NMDAR activation or vehicle control. Only actin^{EGFP} channel is shown. Image width is 20 μm. Graphs show quantification of spine area. *$P<0.05$, **$P<0.01$, ***$P<0.001$ compared with control, K–S test.

LTD on spine size in neurons transfected with W413A-PICK1-IRES-actin^{EGFP}. In neurons expressing control-IRES-actin^{EGFP}, NMDAR activation results in a reduction in spine size (Figure 4C; control + vehicle $1.26 \pm 0.03\,\mu m^2$, control + NMDA $1.10 \pm 0.02\,\mu m^2$, $P<0.001$), which is completely blocked in neurons expressing W413A-PICK1-IRES-EGFP (Figure 4C; W413A-PICK1 + vehicle $1.41 \pm 0.03\,\mu m^2$, W413A-PICK1 + NMDA $1.40 \pm 0.03\,\mu m^2$, $P=0.737$).

To explore the role of endogenous PICK1 expression in NMDA-induced spine shrinkage, we used shRNA to knock down PICK1 expression levels. In control neurons expressing mCherry and actin^{EGFP}, NMDAR activation causes spine shrinkage (Figure 4D; control + vehicle $1.21 \pm 0.04\,\mu m^2$, control + NMDA $0.94 \pm 0.03\,\mu m^2$, $P<0.001$) whereas in neurons expressing reduced levels of endogenous PICK1 following transfection with PICK1 shRNA–mCherry and actin^{EGFP}, spine shrinkage was completely blocked (Figure 4D; shRNA + vehicle $1.31 \pm 0.04\,\mu m^2$, shRNA + NMDA $1.42 \pm 0.05\,\mu m^2$, $P=0.925$).

To further examine the role of PICK1 in NMDA-induced spine shrinkage, we carried out time lapse live cell imaging. For these experiments, we used mCherry as the morphological marker. Mean spine size in control neurons exposed to vehicle was stable throughout the experiment (1 h; Figure 5).

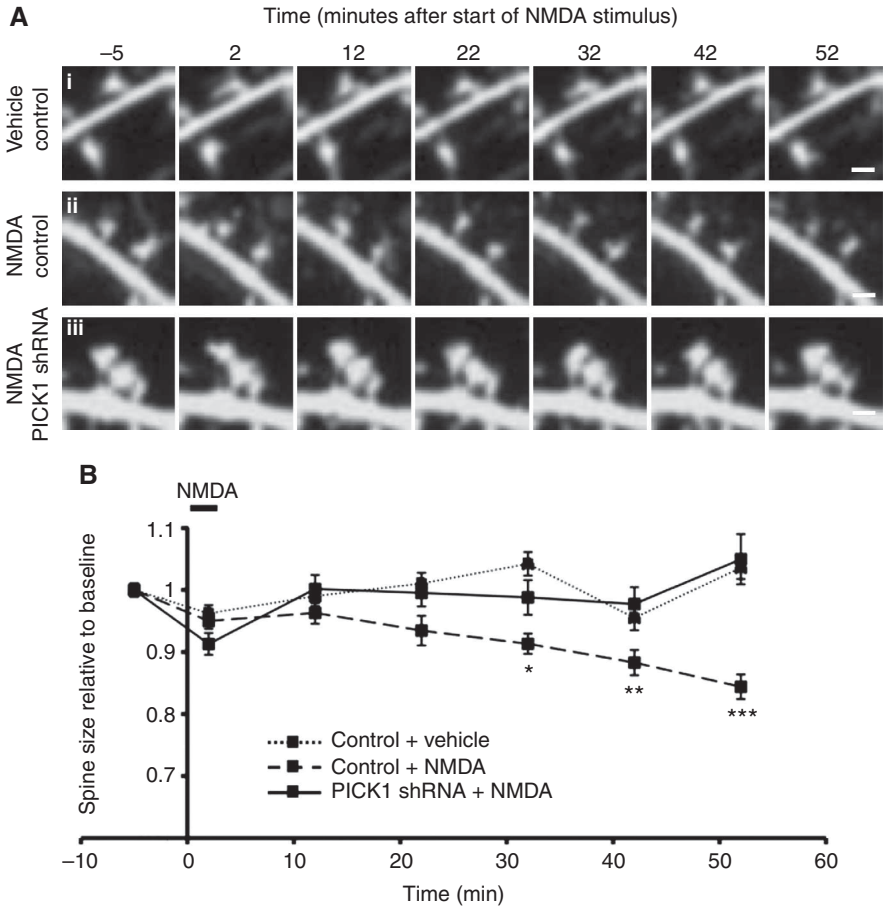

Figure 5 PICK1 knockdown blocks spine shrinkage following NMDAR activation recorded by time lapse live cell imaging. (**A**) Representative images acquired at time points shown relative to the end of chem-LTD stimulus. (i) Spine size is unchanged in the absence of stimulus for the duration of the experiment in neurons transfected with mCherry control. (ii) Chem-LTD leads to spine shrinkage in neurons transfected with control-mCherry. (iii) Chem-LTD-induced spine shrinkage is blocked in neurons transfected with PICK1 shRNA–mCherry. Scale bar: 1 μm. (**B**) Pooled data for live imaging experiments. Spine size is normalised to the baseline value for each recording. Data are from 10–15 neurons, 180–192 spines per condition. $*P<0.05$, $**P<0.001$, $***P<0.0001$ (shRNA + NMDA compared with control + NMDA).

NMDAR activation results in a steady reduction in spine size, and spines were 19% smaller than vehicle-treated controls at 52 min after the start of the stimulus (Figure 5; control + vehicle 1.036 ± 0.02 relative to baseline, control + NMDA 0.84 ± 0.02 relative to baseline, $P<0.0001$), which is consistent with our data from fixed cells. Further analysis revealed that baseline spine size does not influence the extent of shrinkage. Knockdown of endogenous PICK1 by shRNA completely blocks spine shrinkage in response to NMDAR activation (Figure 5; shRNA + NMDA 1.05 ± 0.04 relative to baseline, $P<0.0001$ compared with control + NMDA at 52 min).

These experiments demonstrate a crucial role for PICK1 in mediating LTD-induced spine shrinkage via its interaction with the actin-nucleating Arp2/3 complex.

PICK1–Arp2/3 interactions are involved in synaptically induced LTD in hippocampal CA1 region

As Arp2/3 inhibition by PICK1 is involved in both AMPAR internalisation (Rocca *et al*, 2008) and spine shrinkage (this study) during chemical LTD in dissociated cultures, we investigated the role of this pathway in synaptically induced LTD in CA1 region of hippocampal slices. Hippocampal LTD involves PICK1-mediated internalisation of GluA2-containing AMPARs (Kim *et al*, 2001; Seidenman *et al*, 2003; Terashima *et al*, 2008), but it is unknown whether Arp2/3 regulation by PICK1 is required.

We used viral transduction with IRES-EGFP constructs in acute hippocampal slices cultured for 24 h to allow protein expression. Control neurons expressing EGFP exhibit robust pathway-specific LTD in response to low-frequency stimulation (Figure 6A; control $80.7 \pm 2.7\%$ versus test $59.9 \pm 6.0\%$, $P<0.01$). In contrast, LTD was completely absent in neurons transduced with WT-PICK1-IRES-EGFP (Figure 6B; control $88.6 \pm 3.9\%$ versus test $85.2 \pm 8.1\%$, $P=0.62$). As overexpression of WT-PICK1 reduces surface GluA2, and LTD in CA1 pyramidal neurons involves PICK1-mediated internalisation of GluA2-containing AMPARs, the absence of LTD in WT-PICK1 overexpressing neurons represents an occlusion rather than a block *per se*. Indeed, a previous report found that overexpression of WT-PICK1 reduces surface GluA2, leading to a compensatory increase in synaptic GluA2-lacking AMPARs that are inwardly rectifying and have a larger single-channel conductance than GluA2-containing AMPARs (Terashima *et al*, 2004). We confirmed this effect on basal transmission and found larger, inwardly rectifying AMPAR EPSCs in neurons transduced with WT-PICK1-IRES-EGFP virus compared with neighbouring control neurons

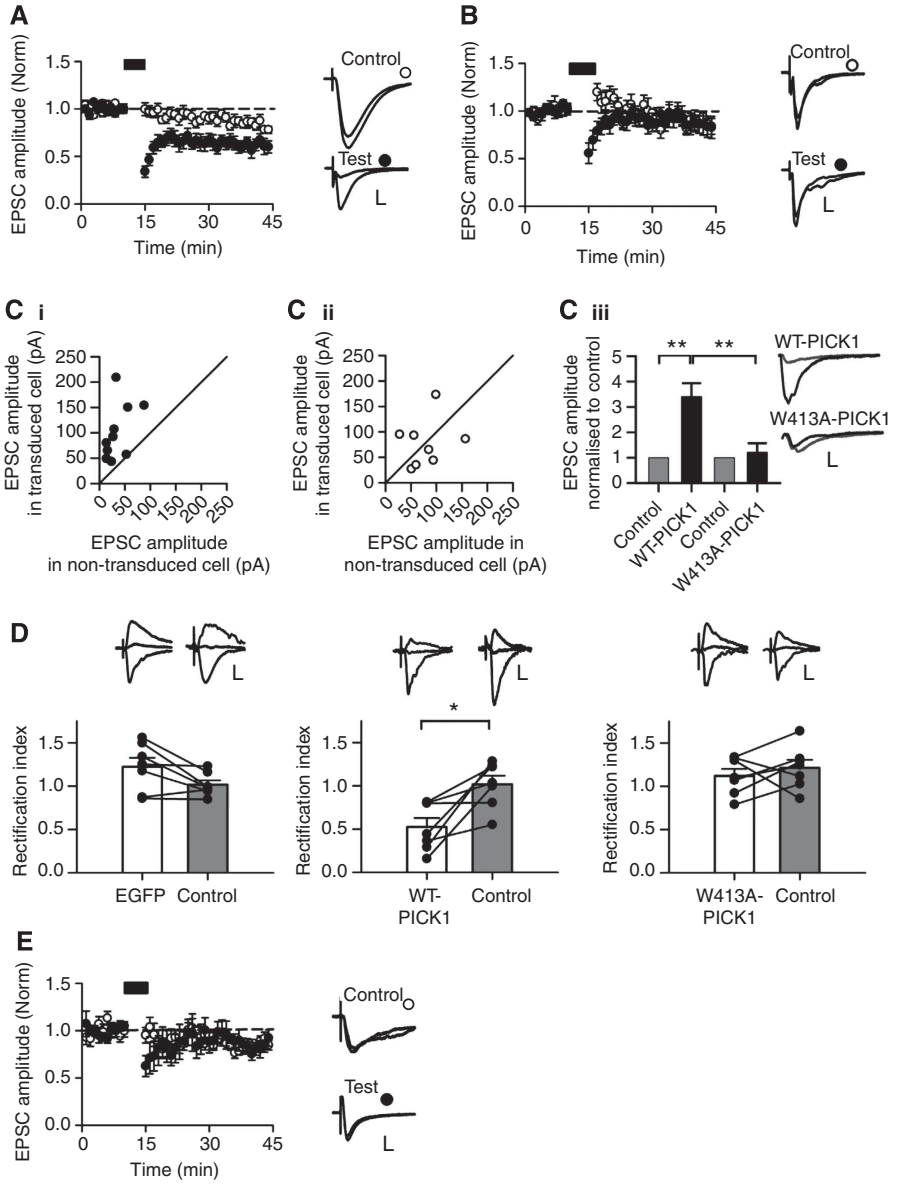

Figure 6 Regulation of hippocampal LTD by PICK1 requires its interaction with the Arp2/3 complex. (**A**) Pooled data of normalised EPSC amplitude versus time for two-pathway LTD experiments from EGFP transduced CA1 neurons. Points represent minute averages of responses from test (filled circles) and control (hollow circles) pathways. Black bar: LTD induction. Example traces were recorded during baseline and 26–30 min after LTD induction in control and test pathways. ± s.e.m. ($n = 11$). Scale bars: control 50 pA/10 ms, test 25 pA/10 ms. (**B**) Pooled data of normalised EPSC amplitude versus time for two-pathway LTD experiments as above, except recorded from WT-PICK1 transduced CA1 neurons ($n = 9$). Scale bars: control 25 pA/10 ms, test 50 pA/10 ms. (**Ci**) EPSC amplitudes of neurons transduced with WT-PICK1-IRES-EGFP versus neighbouring non-transduced cells. Circles represent recordings from a transduced and neighbouring non-transduced cell using the same presynaptic stimulation, $n = 10$. Solid line is unity. (**Cii**) EPSC amplitudes of neurons transduced with W413A-PICK1-IRES-EGFP versus neighbouring non-transduced cells. Circles represent recordings from a transduced and neighbouring non-transduced cell using the same presynaptic stimulation, $n = 8$. Solid line is unity. (**Ciii**) EPSC amplitude in WT-PICK1 and W413A-PICK1 transduced cells normalised to neighbouring non-transduced control cells. $^{**}P < 0.005$. Example traces from transduced (black) and non-transduced control (gray) cells. Scale bars: 100 pA/10 ms. (**D**) Rectification indices of transduced versus neighbouring non-transduced cells. Bars represent mean ± s.e.m., lines represent individual cells ($n = 7$ per condition). $^{*}P < 0.05$. (Top) Example traces recorded at −70, 0 and +40 mV. Scale bars: EGFP: control 15 pA/20 ms, transduced 50 pA/20 ms, WT-PICK1: control 50 pA/20 ms, transduced 20 pA/20 ms, W413A-PICK1: control 20 pA/20 ms, transduced 20 pA/20 ms. (**E**) Pooled data of normalised EPSC amplitude versus time for two-pathway LTD experiments as in (**A**), above, except recorded from W413A-PICK1 transduced neurons ($n = 7$). Scale bars: control 20 pA/20 ms, test 20 pA/20 ms.

(Figure 6C and D). In contrast, neurons expressing the Arp2/3 non-binding mutant, W413A-PICK1, showed no change in AMPAR EPSC amplitude, and no change in rectification index, indicating that interaction with Arp2/3 is essential for PICK1-mediated regulation of basal synaptic transmission (Figure 6C and D). Importantly, in neurons expressing W413A-PICK1, LTD was completely absent (Figure 6E; control 86.1 ± 3.9% versus test 82.5 ± 5.5%, $P = 0.59$). Since basal AMPAR EPSCs in W413A-PICK1 expressing neurons are unchanged compared with controls prior to LTD induction, this effect represents a blockade of plasticity. These experiments indicate that the regulation of Arp2/3-mediated actin polymerisation by PICK1 is required for LTD in the hippocampus.

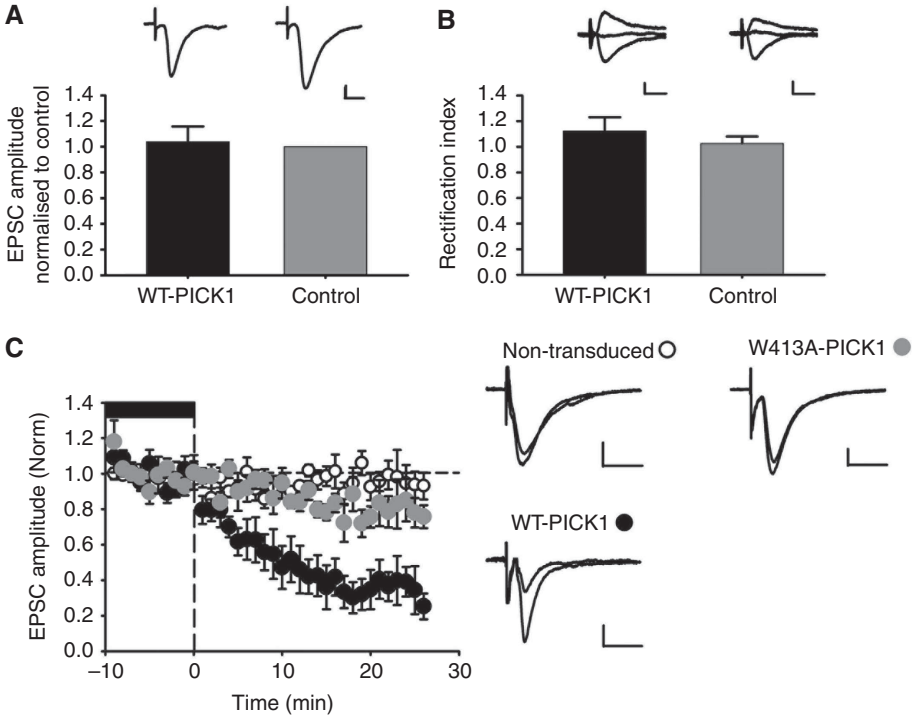

Figure 7 NMDA-dependent synaptic depression induced by PICK1 overexpression requires its interaction with the Arp2/3 complex. (**A**) PICK1 overexpressing neurons in hippocampal slices incubated in D-AP5 have EPSC amplitudes unchanged compared with controls. EPSC amplitudes in WT-PICK1 transduced cells normalised to neighbouring non-transduced control cells ($n=4$). Example traces of WT-PICK1 transduced (black) and non-transduced control (gray) cells. Scale bars: 20 pA/20 ms. (**B**) PICK1 overexpressing neurons in hippocampal slices incubated in D-AP5 are non-rectifying. Rectification indices of WT-PICK1 transduced compared with neighbouring non-transduced control cells ($n=4$). Bars represent mean ± s.e.m. Example traces recorded at −70, 0 and +40 mV. Scale bars: 20 pA/20 ms. (**C**) Washout of D-AP5 results in a rapid reduction in EPSC amplitude in WT-PICK1 overexpressing cells, but not in W413A-PICK1 overexpressing cells. Pooled data of normalised EPSC amplitude versus time for D-AP5 washout experiments from CA1 neurons. Points represent minute averages of responses from WT-PICK1 transduced (black circles, $n=6$), W413A transduced (gray circles, $n=5$) and non-transduced control cells (open circles, $n=6$). Baseline recorded in 50 μM D-AP5 is indicated by the black bar. Example traces were recorded during baseline and 21–25 min following D-AP5 washout. ± s.e.m. Scale bars: 10 pA/20 ms.

To provide further evidence that PICK1–Arp2/3 interactions are required for NMDAR-dependent synaptic depression in the hippocampus, we exploited the fact that the effects of PICK1 overexpression on AMPAR trafficking and EPSC properties are abolished when NMDARs are blocked (Hanley and Henley, 2005; Terashima *et al*, 2008). Neurons transduced with WT-PICK1-IRES-EGFP virus in hippocampal slices and incubated in the NMDAR antagonist D-AP5 from the time of viral transduction have non-rectifying EPSCs with a similar amplitude to non-transduced cells (Figure 7A and B, also see Terashima *et al*, 2008). We are therefore able to investigate the acute effects of altered PICK1 expression by analysing the effects of D-AP5 washout on AMPAR EPSCs. Washout of D-AP5 (therefore activation of NMDARs) leads to a very rapid reduction in AMPAR EPSC amplitude, which is completely blocked by the W413A mutation (Figure 7C). This result demonstrates that the W413A mutation that abolishes the interaction between PICK1 and Arp2/3 blocks synaptic depression in response to NMDAR activation, strongly supporting a role for PICK1-mediated Arp2/3 regulation in the expression of synaptic plasticity.

PICK1–Arp2/3 interaction is enhanced by NMDAR activation

Our data demonstrate a role for the PICK1-mediated inhibition of Arp2/3 activity in NMDA-dependent structural and functional plasticity in hippocampal neurons, suggesting that the PICK1–Arp2/3 interaction may be regulated by NMDAR activity. To test this idea, we carried out co-immunoprecipitations (co-IPs) using an Arp2/3 antibody from hippocampal neuronal cultures at various time points following treatment with a chemical LTD protocol. Figure 8A demonstrates that the interaction between PICK1 and the Arp2/3 complex is significantly increased 10 min after the start of the NMDA stimulus, and returns to basal levels at 20 min. The total amount of PICK1 and Arp2/3 in the lysates is unchanged across all conditions. This shows that following chemical LTD induction, PICK1–Arp2/3 interactions are transiently enhanced, strongly suggesting an increase in PICK1-mediated Arp2/3 inhibition during LTD.

We previously demonstrated that PICK1 functions as a calcium sensor, and that its interaction with AMPAR subunit GluA2 is directly sensitive to calcium in the low micromolar range (Hanley and Henley, 2005). Since NMDAR activation enhances PICK1–Arp2/3 binding, we investigated the possibility that calcium directly regulates this interaction, and carried out co-IPs in buffers containing a range of free calcium concentrations. Figure 8B shows that PICK1 binds the Arp2/3 complex independent of calcium concentration, indicating that an alternative signalling pathway is involved downstream of NMDAR activation to regulate PICK1–Arp2/3 binding.

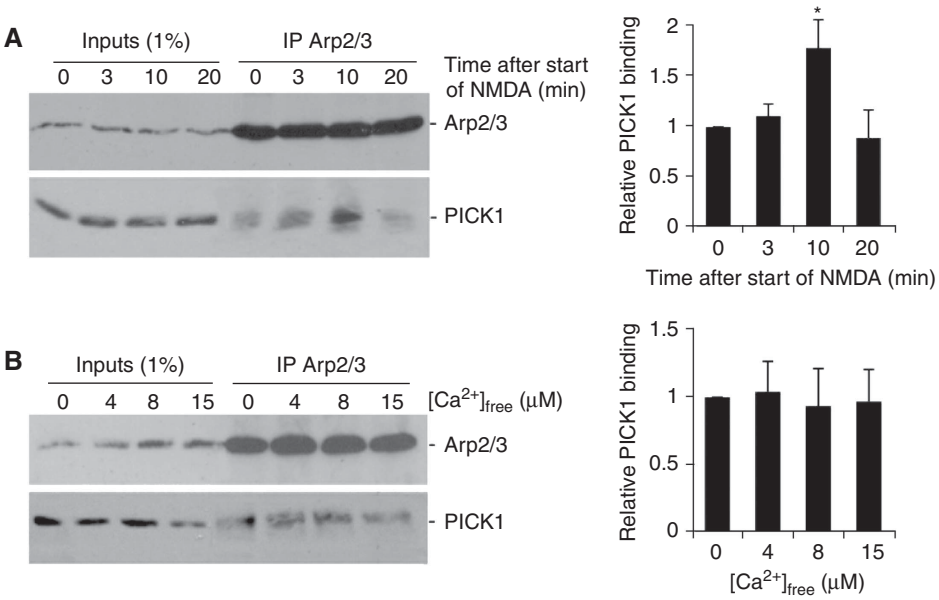

Figure 8 PICK1–Arp2/3 binding is regulated by NMDAR activation, but is not directly sensitive to calcium concentration. (**A**) PICK1–Arp2/3 binding is transiently enhanced 10 min following NMDAR activation. Hippocampal cultures were treated with a 2-min chem-LTD stimulus, then returned to normal medium for the times shown. Lysates from these cultures were immunoprecipitated with anti-p34 antibody (p34 is a subunit of the Arp2/3 complex), and bound proteins detected by western blotting. Graphs show pooled data, $n = 6$. $^*P < 0.05$. (**B**) PICK1–Arp2/3 interaction is not directly sensitive to $[Ca^{2+}]$. Lysates from hippocampal cultures were immunoprecipitated with anti-p34 antibody in buffers containing a range of $[Ca^{2+}]_{free}$ as shown. Bound proteins were detected by western blotting. Graphs show pooled data, $n = 6$.

Discussion

We have defined a role for PICK1 in regulating dendritic spine size via its interaction with the Arp2/3 complex. Knockdown of endogenous PICK1 results in larger spines, indicating that PICK1 functions to restrict spine size under basal conditions. During chemical LTD, spines shrink via a mechanism that requires PICK1 and its interaction with Arp2/3. Since PICK1 inhibits Arp2/3-mediated actin polymerisation (Rocca *et al*, 2008), our data strongly suggest that PICK1 inhibits the Arp2/3 complex in spines resulting in reduced levels of F-actin and consequent shrinkage of spines. We have demonstrated this by using the single amino-acid mutation in PICK1 (W413A) that abolishes Arp2/3 interactions, but has no effect on PICK1 binding to GluA2, GRIP, PKC, Actin, α/β-SNAP or phospholipids (Rocca *et al*, 2008). In addition, we used an independent inhibitor of Arp2/3 activity, N-WASP CA domain (Rohatgi *et al*, 1999; Haeckel *et al*, 2008), and demonstrated that expression of this peptide in neurons mimics and occludes spine shrinkage by PICK1.

We have demonstrated a blockade of NMDA-induced spine shrinkage by overexpression of a dominant-negative PICK1 (W413A) that cannot bind the Arp2/3 complex, and also by reducing endogenous PICK1 expression using shRNA. This is, to our knowledge, the first study that defines a role for a direct inhibitor of the Arp2/3 complex in the regulation of dendritic spine size.

It is noteworthy that neither PICK1 manipulation nor our chemical LTD stimulus affects the density of spines on the dendrite. In addition, no spines completely retract during our live imaging experiments. While a reduction in spine density during hippocampal LTD has been observed, the incidence of spine elimination is very low and is also slow, taking at least an hour following stimulation (Nagerl *et al*, 2004; Zhou *et al*, 2004).

We have also demonstrated that PICK1–Arp2/3 interactions are required for CA3–CA1 LTD in hippocampal slices. With respect to their effect on LTD expression, both WT-PICK1 and W413A-PICK1 overexpressing neurons appear to show the same phenotype. However, under basal conditions, WT-PICK1 overexpression results in larger AMPAR-mediated EPSCs, which occurs as a result of increased high-conductance GluA2-lacking AMPARs at the synapse following PICK1-mediated GluA2 internalisation (Terashima *et al*, 2004). Hippocampal LTD involves PICK1-mediated internalisation of GluA2-containing AMPARs (Kim *et al*, 2001; Seidenman *et al*, 2003; Terashima *et al*, 2008). Therefore, from a GluA2 trafficking perspective, WT-PICK1 overexpression mimics and occludes the subsequent LTD. In contrast, W413A-PICK1 has no influence on basal EPSCs, indicating that neurons expressing this protein have normal levels of synaptic GluA2. W413A-PICK1 subsequently blocks AMPAR internalisation and LTD. Since AMPAR regulation by PICK1 is NMDAR dependent (Hanley and Henley, 2005; Terashima *et al*, 2008), NMDAR blockade using the antagonist D-AP5 suppresses the effect of PICK1 overexpression on basal AMPAR EPSCs. Subsequent withdrawal of D-AP5 results in NMDAR activation, and a PICK1-dependent depression of AMPAR EPSC amplitude, which is abolished by mutating the Arp2/3-binding site on PICK1. We have therefore demonstrated, under both basal and LTD stimulating conditions, that PICK1-mediated, NMDAR-dependent synaptic depression in hippocampal CA1 neurons requires PICK1–Arp2/3 interactions.

It is interesting that the acute effect (minutes; see Figure 7) of PICK1 recruitment is different from the long-term effect (overnight; see Figure 6 and Terashima *et al*, 2004). The acute effect results in reduced AMPAR EPSC amplitude, indicating an internalisation of GluA1/2 or GluA2/3 receptors.

The long-term effect of PICK1 overexpression results in a selective internalisation of GluA2 subunit and enhanced AMPAR EPSCs (Terashima *et al*, 2004). This suggests that, following the PICK1-dependent internalisation of GluA1/2 or GluA2/3 receptors, GluA2-lacking AMPARs (which have higher conductance) are inserted at later time points.

A role for Arp2/3 inhibition by PICK1 in synaptic plasticity predicts that this protein–protein interaction is regulated in response to a plasticity-inducing stimulus. In agreement with this hypothesis, we show that chemical LTD transiently stimulates increased binding of PICK1 to the Arp2/3 complex at 10 min after stimulus. Although spines continue to shrink past 50 min following chemical LTD stimulus, this process is completely blocked by PICK1 knockdown. This suggests that Arp2/3 inhibition by PICK1 is an absolute requirement for initiating spine shrinkage in response to NMDAR activation, and that additional mechanisms are at play at later time points. In contrast to its interaction with GluA2, the PICK1–Arp2/3 interaction is not directly sensitive to calcium, indicating that NMDAR activation stimulates binding via an alternative signalling pathway.

In conjunction with our previous study (Rocca *et al*, 2008), our data show that the inhibition of Arp2/3 activity by PICK1 is involved in both AMPAR internalisation and spine shrinkage following NMDAR activation, as well as LTD recorded electrophysiologically. PICK1 is therefore central to mechanisms that regulate the processes of both functional and structural plasticity. Importantly, our data show that PICK1-mediated spine shrinkage can occur independently of GluA2 surface removal, indicating that PICK1 regulates spine dynamics via direct modulation of structural F-actin, not as a secondary effect of AMPAR trafficking. We previously demonstrated that Arp2/3 inhibition by PICK1 is dramatically enhanced by its interaction with GluA2 c-terminus, and would therefore be highly localised to the specific AMPAR-containing membrane subdomain being mobilised (Rocca *et al*, 2008). This modulation may underlie a mechanism for PICK1 to separately regulate both spine morphology and AMPAR trafficking via inhibition of Arp2/3-mediated actin polymerisation. We propose a model whereby during LTD, PICK1 strongly inhibits actin polymerisation when bound to GluA2 to drive the removal of surface AMPARs, and independently has a less localised effect on F-actin levels to shrink spines. The separate PICK1-dependent pathways controlling spines and AMPAR trafficking are also highlighted by our data that show a lack of involvement of PKC in PICK1-mediated spine shrinkage. This is in contrast to the effect of PICK1 overexpression on AMPAR EPSC properties, which is inhibited by PKC blockade (Terashima *et al*, 2004). In addition to GluA2 and PKC, many other proteins interact with PICK1 (Hanley, 2008), some of which may be involved in the process that leads to spine shrinkage.

We have defined the Arp2/3 inhibitor PICK1 as a novel regulator of dendritic spine dynamics, both in restricting spine size under basal conditions, and in spine shrinkage during plasticity. Furthermore, we have identified important mechanistic details of hippocampal LTD by demonstrating that PICK1 regulates this process via an NMDA-dependent interaction with the Arp2/3 complex. This work shows that PICK1 has a central role not only in regulating AMPAR trafficking and functional plasticity, but also in controlling structural plasticity of dendritic spines by modulating Arp2/3-mediated actin polymerisation.

Materials and methods

Plasmids and plasmid construction

WT-PICK1-IRES-EGFP and W413A-PICK1-IRES-EGFP have been reported previously (Rocca *et al*, 2008). IRES-actin^{EGFP} constructs were constructed by subcloning PICK1 cDNA, IRES cassette and actin^{EGFP} cDNA into pcDNA3.1. shRNA and mCherry reporters were expressed from a modified pFIV (System Biosciences). mCherry was driven by the CaMKII promoter, shRNA by the H1 RNA pol III promoter. The DNA sequence used to express PICK1 shRNA was as follows: 5′AGGATGCTCAGAACCTGATTGTTCAAGAGACAATCAGGT TCTGAGCATCCT3′. The control construct did not contain shRNA. For rescue experiments, WT-PICK1, and W413A-PICK1 had silent mutations: GAc GCa CAa AAt CTa ATc (mutations in lower case). mCherry–CA was constructed by subcloning cDNA corresponding to N-WASP amino acids 459–501 into a modified pcDNA3.1-mCherry to make an mCherry–CA fusion protein.

Antibodies

The following antibodies are used: anti-GluA2 (Millipore), anti-GFP (Alexa 488-conjugated; Invitrogen), anti-tubulin (Sigma), anti-p34 (Arp2/3 complex; Millipore) and anti-PICK1 (NeuroMab).

Hippocampal slice culture and viral transduction

Slices were prepared and maintained overnight essentially as described (Terashima *et al*, 2004, 2008). Transverse 300 μm hippocampal slices were prepared from 14-day-old Wistar rat pups in high Mg ACSF (mM): 119 NaCl, 2.5 KCl, 1 $NaH_2PO_4.H_2O$, 26.2 $NaHCO_3$, 11 glucose, 9 $MgSO_4$ and 2.5 $CaCl_2$ saturated with 95% O_2, 5% CO_2. Slices were transferred to tissue culture inserts (Millicell-CM, 0.4 μm pore size) with sterile MEM (Gibco) containing (mM): 5 $NaHCO_3$, 30 HEPES, 1 Glutamine, 1 $CaCl_2$, 2 $MgSO_4$, 13 Glucose and 20% Horse Serum adjusted to pH 7.28 with NaOH and ~320mOsM. Slices were rested in an incubator at 35°C and 5% CO_2 for 1 h before being pressure injected with Sindbis virus at multiple sites along the CA1 pyramidal cell layer. Slices were returned to the incubator for 24 h before use.

Neuronal culture, transfection and chemical LTD

Hippocampal neurons prepared from E18 Wistar rats were transfected at DIV 12–13 using Lipofectamine 2000, and used for experiments 5–6 days later. For fixed-cell experiments, cultures were fixed in 4% formaldehyde, permeablised, and the GFP signal enhanced by Alexa 488-conjugated anti-GFP. Chem-LTD was induced at 37°C by exposing cells to 0.5 μM TTX in culture medium for 10 min, then transferring coverslips to HBS buffer (20 mM HEPES, pH 7.6, 140 mM NaCl, 5 mM KCl, 1.8 mM $CaCl_2$, 0.8 mM $MgCl_2$ 5 mM glucose, 0.5 μM TTX), followed by a brief application of 20 μM NMDA, 20 μM glycine in the same buffer for 3 min. Cells were washed twice with HBS, and transferred back to original culture medium containing 0.5 μM TTX for 40 min before fixation.

Image acquisition and analysis

Fixed-cell images were acquired using a Zeiss LSM510 confocal microscope. *Z*-stacks of 6–12 images were taken at 2048 × 2048 resolution, optical slice depth of 1 μm per image, and *z*-step of 0.37 μm. At the time of acquisition, laser power was adjusted so that all spines were below the threshold of saturation. Analysis was by ImageJ software (NIH). Maximum intensity projections were processed to smooth contours and a binary mask was obtained after edge detection. The cross-sectional area, and number of spines was calculated. For each condition, 90–100 μm sections of secondary dendrite from each neuron were analysed, 4–6 neurons per experiment, from three separate experiments, resulting in 700–1400 spines per condition. Experiments were both imaged and analysed with the experimenter blind to the experimental conditions. Statistical analyses were performed in Excel (Microsoft). The Student's *t*-test was performed on spine density data. Cumulative plots were analysed using Kolmogorov–Smirnov test (K–S test).

Time lapse live confocal images of dendritic spines were acquired using a Nikon Eclipse Ti-E microscope. *Z*-stacks of 15–20 images were taken at various time points at 512 × 512

resolution with a *z*-step size of 0.4 μm. Neurons were continually perfused at 35°C with HBS at a flow rate of 4 ml/min. For chem-LTD, buffer was switched to HBS containing 20 μM NMDA and 20 μM glycine for 3 min, followed by return to normal HBS. For PMA treatment, perfusion buffer was HBS containing 50 μM D-AP5, 5 μM NBQX and 0.5 μM PMA. Baseline perfusion buffer was the same minus PMA. Glutamate receptor antagonists were present to prevent any PKC-stimulated release of endogenous glutamate from activating postsynaptic glutamate receptors (Calabrese and Halpain, 2005). Analysis was by ImageJ. Maximum intensity projections were produced for each time point and the images were processed and analysed as above.

Measurement of spine length

To determine spine length, *z*-stack images were imported into NeuronStudio (Rodriguez *et al*, 2008), which allows for the automated detection of dendrites and spines. NeuronStudio then measures the length of individual spines and these data were then imported into Excel for statistical analysis.

Surface biotinylation assays

Biotinylations were carried out as described (Hanley and Henley, 2005).

Co-immunoprecipitations

For NMDA-dependent co-IPs, cultured neurons were subjected to the chem-LTD protocol (see above sections), and then returned to HBS for varying time points. Times stated are from the beginning of chem-LTD. Cultures were chilled on ice, then lysed in 125 mM NaCl, 25 mM HEPES pH 7.5, 0.5% Triton X-100, plus protease inhibitors. Lysates were cleared by centrifugation, then incubated with 2 μg anti-p34 antibody for 2 h on ice. Protein A-sepharose beads were added and rotated at 4°C for 1 h, followed by four to five washes in lysis buffer. Bound proteins were then detected by western blotting.

Calcium-dependent co-IPs were carried out as described (Hanley and Henley, 2005), using 2 μg anti-p34 antibody for the co-IP.

Electrophysiology

Slices were visualised using combined IR/DIC and fluorescence microscopy with an Olympus BX51WI upright microscope. Whole-cell patch-clamp recordings were made from visually identified CA1 pyramidal neurons in overnight cultured, virally transduced hippocampal slices. Recordings were made in ACSF containing the following (mM): 119 NaCl, 2.5 KCl, 1 $NaH_2PO_4.H_2O$, 26.2 $NaHCO_3$, 11 glucose, 1.3 $MgSO_4$, 2.5 $CaCl_2$ and 0.05 picrotoxin saturated with 95% O_2, 5% CO_2. The intracellular solution was composed as follows (mM): 117 $CsMeSO_3$, 8 NaCl, 10 HEPES, 5 QX314, 4 ATP-Mg. 0.3 GTP-Na, 0.5 EGTA adjusted to pH 7.4 with CsOH and ~290 mOsM. For AMPAR rectification measurements, 0.1 mM spermine was added to the intracellular solution and 50 μM D-AP5 to the extracellular solution. In all experiments, the CA3 region was severed from the hippocampal slice prior to placement in the perfusion chamber to minimise recurrent excitation.

Schaffer collateral synaptic pathways were stimulated using two bipolar tungsten electrodes placed in *stratum radiatum* of the CA1 region, one towards CA3 and the other towards the subiculum. For EPSC rectification and amplitude measurements, a fluorescent transduced CA1 pyramidal cell was first identified for recording followed by a neighbouring non-transduced cell. For LTD experiments, individual transduced cells were recorded in each slice. Stable baseline recordings of 10 min were made at a holding potential of −70 mV and a stimulation frequency of 0.1 Hz for each pathway. The LTD induction protocol consisted of 300 stimuli at 1 Hz given to the test pathway while holding the membrane potential at −40 mV. LTD was assessed 26–30 min after the induction protocol by statistical comparison between control and test pathways (paired Student's *t*-test).

EPSC amplitudes were measured at a holding potential of −70 mV, EPSC rectification at holding potentials of −70 mV, 0 mV and +40 mV. For rectification analysis, a ratio of the I/V plot slopes between −70 mV and 0 mV and between 0 mV and +40 mV data was calculated to generate a rectification index ($RI = Gradient_{+40\,mV}/Gradient_{-70\,mV}$). EPSC rectification and amplitudes were compared between transduced and non-transduced cells in the same slice (paired Student's *t*-test).

Supplementary data

Supplementary data are available at *The EMBO Journal* Online (http://www.embojournal.org).

Acknowledgements

We thank Z Bashir, G Collingridge, M Frerking and K Murk for critical reading of the manuscript; A Matus for $actin^{EGFP}$ plasmid; and P Tidball and P Rubin for technical assistance. JGH is a RCUK fellow. YN, CLW and AP were funded by MRC studentships. This work was funded by The Wellcome Trust and the MRC, and supported by ENI-NET.

Author contributions: YN carried out and analysed biochemistry and most of the imaging experiments. CLW carried out and analysed electrophysiology experiments. APP carried out and analysed electrophysiology experiments. NJ carried out and analysed an imaging experiment. JMH advised on biochemistry and imaging experiments. JRM supervised and advised on electrophysiology experiments. JGH carried out and analysed some imaging experiments, advised on biochemistry and imaging experiments, supervised the project and wrote the paper.

Conflict of interest

The authors declare that they have no conflict of interest.

References

Ackermann M, Matus A (2003) Activity-induced targeting of profilin and stabilization of dendritic spine morphology. *Nat Neurosci* **6:** 1194–1200

Biou V, Bhattacharyya S, Malenka RC (2008) Endocytosis and recycling of AMPA receptors lacking GluR2/3. *Proc Natl Acad Sci USA* **105:** 1038–1043

Bloodgood BL, Sabatini BL (2007) Ca(2+) signaling in dendritic spines. *Curr Opin Neurobiol* **17:** 345–351

Calabrese B, Halpain S (2005) Essential role for the PKC target MARCKS in maintaining dendritic spine morphology. *Neuron* **48:** 77–90

Chao HW, Hong CJ, Huang TN, Lin YL, Hsueh YP (2008) SUMOylation of the MAGUK protein CASK regulates dendritic spinogenesis. *J Cell Biol* **182:** 141–155

Cingolani LA, Goda Y (2008) Actin in action: the interplay between the actin cytoskeleton and synaptic efficacy. *Nat Rev Neurosci* **9:** 344–356

Dillon C, Goda Y (2005) The actin cytoskeleton: integrating form and function at the synapse. *Annu Rev Neurosci* **28:** 25–55

Haeckel A, Ahuja R, Gundelfinger ED, Qualmann B, Kessels MM (2008) The actin-binding protein Abp1 controls dendritic spine morphology and is important for spine head and synapse formation. *J Neurosci* **28:** 10031–10044

Hanley JG (2008) PICK1: a multi-talented modulator of AMPA receptor trafficking. *Pharmacol Ther* **118:** 152–160

Hanley JG, Henley JM (2005) PICK1 is a calcium-sensor for NMDA-induced AMPA receptor trafficking. *EMBO J* **24:** 3266–3278

Hering H, Sheng M (2003) Activity-dependent redistribution and essential role of cortactin in dendritic spine morphogenesis. *J Neurosci* **23:** 11759–11769

Hsieh H, Boehm J, Sato C, Iwatsubo T, Tomita T, Sisodia S, Malinow R (2006) AMPAR removal underlies Abeta-induced synaptic depression and dendritic spine loss. *Neuron* **52:** 831–843

Kaksonen M, Toret CP, Drubin DG (2006) Harnessing actin dynamics for clathrin-mediated endocytosis. *Nat Rev Mol Cell Biol* **7:** 404–414

Kennedy MB, Beale HC, Carlisle HJ, Washburn LR (2005) Integration of biochemical signalling in spines. *Nat Rev Neurosci* **6:** 423–434

Kim CH, Chung HJ, Lee HK, Huganir RL (2001) Interaction of the AMPA receptor subunit GluR2/3 with PDZ domains regulates

hippocampal long-term depression. *Proc Natl Acad Sci USA* **98:** 11725–11730

Kim Y, Sung JY, Ceglia I, Lee KW, Ahn JH, Halford JM, Kim AM, Kwak SP, Park JB, Ho Ryu S, Schenck A, Bardoni B, Scott JD, Nairn AC, Greengard P (2006) Phosphorylation of WAVE1 regulates actin polymerization and dendritic spine morphology. *Nature* **442:** 814–817

Lu W, Shi Y, Jackson AC, Bjorgan K, During MJ, Sprengel R, Seeburg PH, Nicoll RA (2009) Subunit composition of synaptic AMPA receptors revealed by a single-cell genetic approach. *Neuron* **62:** 254–268

Matsuzaki M (2007) Factors critical for the plasticity of dendritic spines and memory storage. *Neurosci Res* **57:** 1–9

Merrifield CJ (2004) Seeing is believing: imaging actin dynamics at single sites of endocytosis. *Trends Cell Biol* **14:** 352–358

Nagerl UV, Eberhorn N, Cambridge SB, Bonhoeffer T (2004) Bidirectional activity-dependent morphological plasticity in hippocampal neurons. *Neuron* **44:** 759–767

Okamoto K, Nagai T, Miyawaki A, Hayashi Y (2004) Rapid and persistent modulation of actin dynamics regulates postsynaptic reorganization underlying bidirectional plasticity. *Nat Neurosci* **7:** 1104–1112

Passafaro M, Nakagawa T, Sala C, Sheng M (2003) Induction of dendritic spines by an extracellular domain of AMPA receptor subunit GluR2. *Nature* **424:** 677–681

Perez JL, Khatri L, Chang C, Srivastava S, Osten P, Ziff EB (2001) PICK1 targets activated protein kinase Calpha to AMPA receptor clusters in spines of hippocampal neurons and reduces surface levels of the AMPA-type glutamate receptor subunit 2. *J Neurosci* **21:** 5417–5428

Racz B, Weinberg RJ (2008) Organization of the Arp2/3 complex in hippocampal spines. *J Neurosci* **28:** 5654–5659

Rocca DL, Martin S, Jenkins EL, Hanley JG (2008) Inhibition of Arp2/3-mediated actin polymerization by PICK1 regulates neuronal morphology and AMPA receptor endocytosis. *Nat Cell Biol* **10:** 259–271

Rodriguez A, Ehlenberger DB, Dickstein DL, Hof PR, Wearne SL (2008) Automated three-dimensional detection and shape classification of dendritic spines from fluorescence microscopy images. *PLoS One* **3:** e1997

Rohatgi R, Ma L, Miki H, Lopez M, Kirchhausen T, Takenawa T, Kirschner MW (1999) The interaction between N-WASP and the Arp2/3 complex links Cdc42-dependent signals to actin assembly. *Cell* **97:** 221–231

Saglietti L, Dequidt C, Kamieniarz K, Rousset MC, Valnegri P, Thoumine O, Beretta F, Fagni L, Choquet D, Sala C, Sheng M, Passafaro M (2007) Extracellular interactions between GluR2 and N-cadherin in spine regulation. *Neuron* **54:** 461–477

Saneyoshi T, Wayman G, Fortin D, Davare M, Hoshi N, Nozaki N, Natsume T, Soderling TR (2008) Activity-dependent synaptogenesis: regulation by a CaM-kinase kinase/CaM-kinase I/betaPIX signaling complex. *Neuron* **57:** 94–107

Seidenman KJ, Steinberg JP, Huganir R, Malinow R (2003) Glutamate receptor subunit 2 Serine 880 phosphorylation modulates synaptic transmission and mediates plasticity in CA1 pyramidal cells. *J Neurosci* **23:** 9220–9228

Sekino Y, Kojima N, Shirao T (2007) Role of actin cytoskeleton in dendritic spine morphogenesis. *Neurochem Int* **51:** 92–104

Shepherd JD, Huganir RL (2007) The cell biology of synaptic plasticity: AMPA receptor trafficking. *Annu Rev Cell Dev Biol* **23:** 613–643

Staudinger J, Zhou J, Burgess R, Elledge SJ, Olson EN (1995) PICK1: a perinuclear binding protein and substrate for protein kinase C isolated by the yeast two-hybrid system. *J Cell Biol* **128:** 263–271

Takenawa T, Suetsugu S (2007) The WASP-WAVE protein network: connecting the membrane to the cytoskeleton. *Nat Rev Mol Cell Biol* **8:** 37–48

Terashima A, Cotton L, Dev KK, Meyer G, Zaman S, Duprat F, Henley JM, Collingridge GL, Isaac JT (2004) Regulation of synaptic strength and AMPA receptor subunit composition by PICK1. *J Neurosci* **24:** 5381–5390

Terashima A, Pelkey KA, Rah JC, Suh YH, Roche KW, Collingridge GL, McBain CJ, Isaac JT (2008) An essential role for PICK1 in NMDA receptor-dependent bidirectional synaptic plasticity. *Neuron* **57:** 872–882

Wang XB, Yang Y, Zhou Q (2007) Independent expression of synaptic and morphological plasticity associated with long-term depression. *J Neurosci* **27:** 12419–12429

Wegner AM, Nebhan CA, Hu L, Majumdar D, Meier KM, Weaver AM, Webb DJ (2008) N-WASP and the arp2/3 complex are critical regulators of actin in the development of dendritic spines and synapses. *J Biol Chem* **283:** 15912–15920

Zhou Q, Homma KJ, Poo MM (2004) Shrinkage of dendritic spines associated with long-term depression of hippocampal synapses. *Neuron* **44:** 749–757